

Sampling-Based Motion Planning with Online Racing Line Generation for Autonomous Driving on Three-Dimensional Race Tracks

Levent Ögretmen¹, Matthias Rowold¹, Alexander Langmann², and Boris Lohmann¹

Abstract—Existing approaches to trajectory planning for autonomous racing employ sampling-based methods, generating numerous jerk-optimal trajectories and selecting the most favorable feasible trajectory based on a cost function penalizing deviations from an offline-calculated racing line. While successful on oval tracks, these methods face limitations on complex circuits due to the simplistic geometry of jerk-optimal edges failing to capture the complexity of the racing line. Additionally, they only consider two-dimensional tracks, potentially neglecting or surpassing the actual dynamic potential. In this paper, we present a sampling-based local trajectory planning approach for autonomous racing that can maintain the lap time of the racing line even on complex race tracks and consider the race track’s three-dimensional effects. In simulative experiments, we demonstrate that our approach achieves lower lap times and improved utilization of dynamic limits compared to existing approaches. We also investigate the impact of online racing line generation, in which the time-optimal solution is planned from the current vehicle state for a limited spatial horizon, in contrast to a closed racing line calculated offline. We show that combining the sampling-based planner with the online racing line generation can significantly reduce lap times in multi-vehicle scenarios.

I. INTRODUCTION

Planning for autonomous racing can be broadly divided into two components: global planning, in which a racing line is planned in the absence of opposing vehicles, and local planning, in which the local environment, i.e., opposing vehicles, is considered. The task of local planning is to adhere to the racing line and, when other vehicles are in the vicinity, make deviations as needed to overtake and prevent collisions.

Sampling-based approaches are commonly employed for local planning due to their simplicity and ability to solve the non-convexity of racing scenarios. In these approaches, multiple trajectory candidates are generated by sampling nodes in the spatio-temporal space and a subsequent generation of edges. The individual trajectories are checked for feasibility, and the optimal one is selected based on a predefined cost function. While sampling-based approaches have been successfully applied to oval race tracks [1]–[3], following the racing line on a complex circuit in the presence of opposing vehicles presents greater challenges. Furthermore, the existing approaches are limited to two-dimensional



Fig. 1. The race cars of the TUM Autonomous Motorsport (right) and Cavalier (left) teams in a banked turn on the Las Vegas Motor Speedway.

(2D) race tracks. However, including three-dimensional (3D) aspects is essential to navigate effectively through elevation changes, banked curves, and various track features. Ignoring these 3D elements can lead to suboptimal racing performance and hinder the ability to exploit advantageous trajectories on the race track. The racing line from global planning entering the cost function is calculated offline in previous approaches due to the required computation times. However, deviations from the racing line, which regularly occur, for example, due to overtaking maneuvers, result in the racing line losing its optimality, leading to suboptimal overall performance. Emerging approaches in which the racing line is regenerated online hold the potential to immediately respond to deviations from the racing line.

In this paper, we propose the first sampling-based local planning approach that accounts for 3D effects as they occur on many race tracks, as shown in Fig. 1. We further present an adaptation of the trajectory generation of existing approaches, which is necessary for racing line following on complex circuits, enabling lower lap times. Finally, we evaluate the impact of online racing line generation on the overall performance compared to an offline computed racing line.

A. Related Work

Numerous resources, like [4], provide insights into motion planning for traffic situations. A comprehensive examination of global and local planning techniques for racing scenarios can be located in [5].

Global planning, which involves the generation of a racing line serving as a reference for local planning, can be performed either offline or online. In the offline approach, a closed racing line is generated, where the initial state corresponds to the final state, representing the optimal tra-

¹Levent Ögretmen, Matthias Rowold, and Boris Lohmann are with the Chair of Automatic Control, TUM School of Engineering and Design, Technical University of Munich, Germany

{levent.oegretmen, matthias.rowold, lohmann}@tum.de

²Alexander Langmann is with the Professorship of Autonomous Vehicle Systems, TUM School of Engineering and Design, Technical University of Munich, Germany alexander.langmann@tum.de

jectory for a complete flying lap. Commonly used optimality criteria for generating the racing line include time [6] and curvature optimality [7]. In the online approach, the racing line is regularly re-planned, considering the current vehicle state. Since the computing time must be reduced for the online application, the racing line is not generated for the entire race track but only for a limited horizon, as in [8]. While the aforementioned approach assumes a 2D race track, Rowold et al. [9] perform an online racing line generation considering the effects of a 3D race track. The 3D effects are included by constraining the combined lateral and longitudinal acceleration by diamond-shaped gg-diagrams that depend on both velocity and vertical acceleration.

The racing line serves as a reference for local planning, which additionally considers the local environment. Hence, in the event of a slower opposing vehicle occupying the intended racing line, the ego vehicle must deviate from it. The non-convex nature of such an overtaking scenario presents a significant challenge for local planning. While variational methods that solve an optimal control problem by numerical optimization usually find a local optimum depending on the initialization, approaches exist that select the overtaking direction prior to optimization and perform optimization within a constrained sector [10], [11]. Other approaches, such as [3], [12], are based on spatio-temporal graphs built along the race track. By performing a graph search, the global discrete-optimal solution can be found. However, due to the exponential increase of the computation time with each dimension, only a coarse discretization of the graph is possible, which limits the application to simple race tracks like oval courses.

Further, sampling-based approaches are often used for local planning. While methods that randomly sample in free space, like rapidly exploring random trees (RRTs) [13], are generally not used for racing, several approaches exist that generate multiple trajectories by sampling in spatio-temporal space. In [14], a set of trajectories for two vehicles is generated by sampling, and a non-cooperative, nonzero-sum game is solved. Werling et al. [15] generate multiple trajectories for traffic scenarios using jerk-optimal curves in curvilinear coordinates that connect the vehicle state to the sampled nodes. The individual trajectories are checked for feasibility, and the optimal valid one is selected according to a cost function. Raji et al. [1] use these jerk-optimal curves for racing on oval race tracks. In [2], the jerk-optimal edges are used to generate the initial edges connecting the vehicle state to a coarse spatio-temporal graph computed offline. The mentioned approaches based on the generation of jerk-optimal curves in curvilinear coordinates are characterized by low computational cost, flexibility in the cost function design, and the ability to resolve non-convexity. However, the jerk-optimal motion primitives are simple in structure and cannot represent complex geometries. This makes it difficult to track the racing line for complex race tracks, so the approaches have been limited to oval race tracks or road traffic. Moreover, none of the mentioned approaches can account for the 3D effects of a race track.

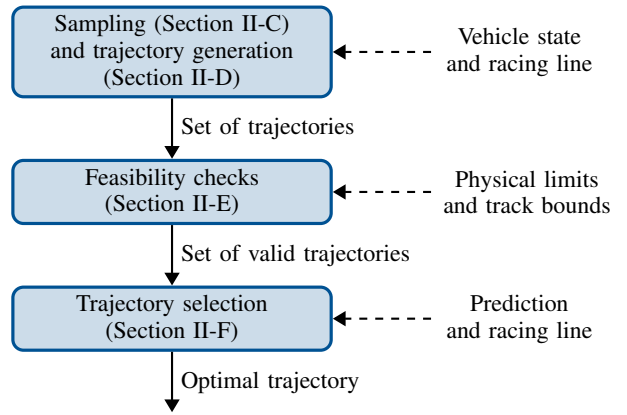


Fig. 2. Structure of our local planning approach with all needed inputs.

B. Contribution

This paper proposes a novel sampling-based local trajectory planning approach for complex 3D race tracks. We further investigate the effect of online racing line generation on the overall performance. The main contributions can be summarized as follows:

- We show that the jerk-optimal trajectory generation used in existing sampling-based planning approaches is sufficient for oval race tracks but unsuitable for complex ones. We adapt the trajectory generation such that the racing line can also be followed on more complex race tracks.
- We propose a method for incorporating the 3D effects of the race track into local planning and show its advantages. Our approach constitutes a generalization of the 2D sampling-based approaches mentioned in Section I-A.
- In contrast to existing approaches, we do not rely on a fixed offline computed racing line but on an online racing line generation. We investigate the effect of online generation on the overall performance compared to using an offline computed racing line.

II. METHODOLOGY

Sections II-A and II-B introduce the representation of the 3D race track, the racing line, and all necessary notations. The structure of our local trajectory planning approach is shown in Fig. 2 and also serves as the structure for the remainder of this section. The sampling in spatio-temporal space and the connection of the sampled nodes with the vehicle state are described in Sections II-C and II-D. The feasibility checks of the generated edges follow in Section II-E, and the selection of the optimal trajectory with the associated definition of the cost function in Section II-F.

A. 3D Track Representation

For the 3D race track, we use the representation introduced in [16], which is based on a spine and a lateral offset to it. The spine, referred to in the following as the reference line, is a three-dimensional curve

$$C = \{c(s) \in \mathbb{R}^3 \mid s \in [0, s_f]\} \quad (1)$$

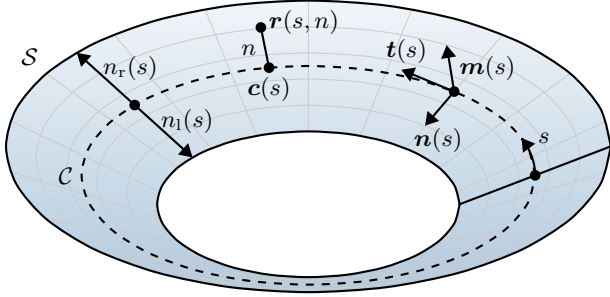


Fig. 3. Representation of a closed, counterclockwise orientated 3D race track with negative banking ($\varphi < 0$) and without slope ($\mu = 0$).

parameterized with respect to its arc length s . Since we are specifically considering closed race tracks, it holds that $\mathbf{c}(0) = \mathbf{c}(s_f)$. We now introduce a moving coordinate system associated with the reference line \mathcal{C} , as depicted in Fig. 3. This coordinate system, which we refer to as the road frame, is spanned by the three unit vectors $\mathbf{t}(s)$, $\mathbf{n}(s)$, and $\mathbf{m}(s)$. The unit vector $\mathbf{t}(s) = \frac{d\mathbf{c}(s)}{ds}$ is tangential to the reference line \mathcal{C} . $\mathbf{n}(s)$ is orthogonal to $\mathbf{t}(s)$ and lies in the plane of the race track. The road frame is completed with $\mathbf{m}(s) = \mathbf{t}(s) \times \mathbf{n}(s)$, which is thus orthogonal. The orientation of the coordinate system is expressed by intrinsic zyx Euler angles, where $\theta(s)$, $\mu(s)$, and $\varphi(s)$ refer to the rotations around the corresponding axes. The angular velocity of the road frame with respect to the arc length s is denoted as $\mathbf{\Omega}(s) = [\Omega_x(s) \ \Omega_y(s) \ \Omega_z(s)]^\top$ and can be derived from the derivatives of the Euler angles [9]. Given the width between the reference line and the left and right track boundaries $n_l(s)$ and $n_r(s)$, the race track surface \mathcal{S} can now be defined as:

$$\mathcal{S} = \{ \mathbf{r}(s, n) = \mathbf{c}(s) + \mathbf{n}(s) \cdot n \in \mathbb{R}^3 \mid s \in [0, s_f], n \in [n_r(s), n_l(s)] \}. \quad (2)$$

While s represents the progress along the reference line of length s_f , n corresponds to the lateral offset on the plane of the race track relative to the reference line.

B. Racing Line

The racing line \mathcal{R} with a fixed spatial horizon H_{rl} and a respective time horizon T_{rl} is given as a curve parameterized with respect to time t in curvilinear coordinates:

$$\mathcal{R} = \{ (s_{rl}(t), n_{rl}(t)) \mid t \in [0, T_{rl}] \}. \quad (3)$$

We assume here that the racing line originates at the current longitudinal vehicle position s_0 , i.e., $s_{rl}(0) = s_0$ holds. The sampling in Section II-C and the trajectory generation in Section II-D are performed depending on $s_{rl}(t)$, $n_{rl}(t)$, and their temporal derivatives $\dot{s}_{rl}(t)$, $\ddot{s}_{rl}(t)$, $\dot{n}_{rl}(t)$, and $\ddot{n}_{rl}(t)$ to generate trajectories with a tendency towards the racing line. However, it should also be possible to follow the path of the racing line with a longitudinal profile $s(t)$ deviating from $s_{rl}(t)$, e.g., in case of a braking maneuver. In this case, the lateral profile $n_{rl}(t)$ is traversed with a different temporal profile, which requires adjustment of its time derivatives.

For a given longitudinal curve $s_i(t)$, the lateral profile $\tilde{n}_{rl,i}(t)$ required to replicate the path of the racing line can be stated as the function composition $\tilde{n}_{rl,i}(t) = n_{rl}(s_{rl}^{-1}(s_i(t)))$. Applying the chain and inverse function rules to the emergent derivatives of the inverse function $s_{rl}^{-1}(s_i(t))$, we obtain the time derivatives, omitting the arguments for brevity:

$$\dot{\tilde{n}}_{rl,i} = \frac{\dot{n}_{rl}}{\dot{s}_{rl}} \cdot \dot{s}_i, \quad (4a)$$

$$\ddot{\tilde{n}}_{rl,i} = \left(\frac{\ddot{n}_{rl}}{\dot{s}_{rl}^2} - \frac{\dot{n}_{rl}\ddot{s}_{rl}}{\dot{s}_{rl}^3} \right) \cdot \dot{s}_i^2 + \frac{\dot{n}_{rl}}{\dot{s}_{rl}} \cdot \ddot{s}_i. \quad (4b)$$

C. Sampling in Curvilinear Coordinates

Given the vehicle state $S_0 = [s_0, \dot{s}_0, \ddot{s}_0, n_0, \dot{n}_0, \ddot{n}_0]$, we sample end nodes $S_{e,i,j} = [\dot{s}_{e,i}, \ddot{s}_{e,i}, n_{e,j}, \dot{n}_{e,j}, \ddot{n}_{e,j}]$ and then connect S_0 to the sampled nodes $S_{e,i,j}$ with a fixed horizon T , resulting in a set of trajectories. As the computational cost increases exponentially with each dimension, not all quantities are sampled in $S_{e,i,j}$, but only the longitudinal velocity $\dot{s}_{e,i}$ and the lateral position $n_{e,j}$. The higher-order derivatives, on the other hand, are selected appropriately without further sampling, as explained below. Moreover, $S_{e,i,j}$ does not include a longitudinal end position, as in the racing scenario the selected end velocities $\dot{s}_{e,i}$ are more decisive and the end positions adjust accordingly.

Since an essential task of local planning is to follow the racing line \mathcal{R} , the sampled nodes $S_{e,i,j}$ must be chosen so that the resulting trajectories can represent the racing line. In the longitudinal direction, $N_{\dot{s}}$ equidistantly distributed samples are generated in the interval $\dot{s}_{e,i} \in [0, \dot{s}_{rl}(T) \cdot K_{\dot{s}}]$, additionally always including the terminal racing line velocity $\dot{s}_{rl}(T)$. The enlargement of the range by $K_{\dot{s}} > 1$ is required to allow for possible necessary deviation from the racing line. The acceleration $\ddot{s}_{e,i}$ associated with the sampled $\dot{s}_{e,i}$ is chosen to be $\ddot{s}_{rl}(T)$ to allow tracking of the racing line. However, to obtain reasonable trajectories also for larger deviations from the racing line, we interpolate linearly between 0 and $\ddot{s}_{rl}(T)$ depending on the proximity of \dot{s}_0 to $\dot{s}_{rl}(0)$ and $\dot{s}_{e,i}$ to $\dot{s}_{rl}(T)$.

Given a longitudinal curve $s_i(t)$, we generate several lateral curves that complement it. For this, we sample N_n equidistantly distributed samples within the track boundaries $n_{e,j} \in [n_r(s_{e,i}) + d_w/2, n_l(s_{e,i}) - d_w/2]$, considering the vehicle width d_w and again including the terminal racing line position $\tilde{n}_{rl,i}(T)$. We select the corresponding time derivatives $\dot{n}_{e,j}$ and $\ddot{n}_{e,j}$ to ensure the alignment at the track boundaries and the racing line and interpolate linearly in between. Note that the lateral samples and curves must be recalculated for each $s_i(t)$, as $\tilde{n}_{rl,i}(t)$ changes accordingly.

D. Trajectory Generation

For trajectory generation, the initial state S_0 is connected to the sampled end nodes $S_{e,i,j}$, and the resulting $s_i(t)$ and $n_j(t)$ pairs are transformed into Cartesian coordinates for the subsequent feasibility checks. First, we examine the creation of jerk-optimal trajectories as described in existing

literature. Following that, we introduce our novel approach to trajectory generation, offering enhanced racing line tracking capabilities on complex race tracks.

As shown in [17], for a point mass, quintic polynomials connecting a start state $[p_0, \dot{p}_0, \ddot{p}_0]$ to an end state $[p_e, \dot{p}_e, \ddot{p}_e]$ with the time horizon T minimize the cost functional

$$J(p(t)) = \frac{1}{2} \int_0^T \ddot{p}^2(t) dt \quad (5)$$

and are therefore jerk-optimal. If p_e is arbitrary, causing the end state to lie on a manifold, quartic polynomials minimize the cost functional (5) as derived in [18]. Applied to our case, quintic polynomials can be used for curve generation in the lateral direction and quartic polynomials in the longitudinal direction. The resulting jerk-optimal curves in curvilinear coordinates reduce abrupt acceleration changes, which has a beneficial effect on the subsequent tracking control as well as vehicle stability and are used in the context of the racing scenario in [1] and [2]. On the other hand, these trajectories exhibit only a simple structure, which generally cannot represent the racing line geometry for a complex race track. This leads to a degraded racing line tracking performance so that the jerk-optimal trajectories can only be applied reasonably for race tracks with simple racing lines that can be approximated well by the polynomials, such as oval race tracks. The racing line tracking in the lateral direction can be improved by selecting a reference line closer to the racing line to be driven. However, such a measure is unsuitable for online racing line generation due to the varying racing line. Moreover, the problem of tracking in the longitudinal direction remains, requiring an adaptation of the trajectory generation.

The main idea is to generate the jerk-optimal curves relative to the racing line and then add the racing line to them. This allows the racing line to be tracked exactly and simultaneously enables smooth jerk-optimal deviations from the racing line, e.g., during overtaking or braking maneuvers. For realization, we subtract the racing line start conditions from the start state

$$\begin{aligned} \tilde{S}_0 = [s_0 - s_{r1}(0), \dot{s}_0 - \dot{s}_{r1}(0), \ddot{s}_0 - \ddot{s}_{r1}(0), \\ n_0 - \tilde{n}_{r1,i}(0), \dot{n}_0 - \dot{\tilde{n}}_{r1,i}(0), \ddot{n}_0 - \ddot{\tilde{n}}_{r1,i}(0)] \end{aligned} \quad (6)$$

and the end conditions from the sampled end state

$$\begin{aligned} \tilde{S}_{e,ij} = [\dot{s}_{e,i} - \dot{s}_{r1}(T), \ddot{s}_{e,i} - \ddot{s}_{r1}(T), n_{e,j} - \tilde{n}_{r1,i}(T), \\ \dot{n}_{e,j} - \dot{\tilde{n}}_{r1,i}(T), \ddot{n}_{e,j} - \ddot{\tilde{n}}_{r1,i}(T)] \end{aligned} \quad (7)$$

and connect the adapted states with the mentioned quartic and quintic polynomials. To comply with the actual start state S_0 and the sampled end states $S_{e,ij}$ specified in Section II-C, the racing line profiles are then added to the resulting curves. Fig. 4 shows exemplarily the comparison of jerk-optimal curves and curves generated relative to the racing line, referred to as relative curves in the following. It shows the tendency of the relative edges to the racing line and that, in contrast to the jerk-optimal curves, the basic geometry of the racing line can be recreated.

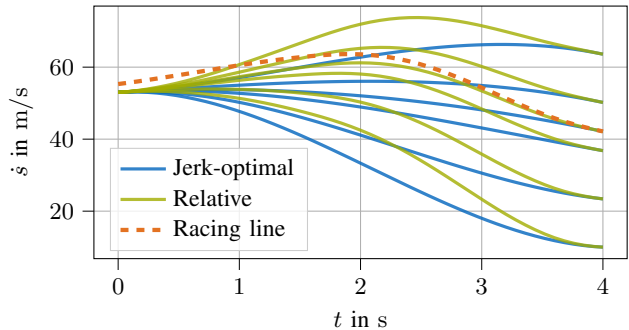


Fig. 4. Comparison of jerk-optimal and relative trajectory generation with $\dot{s}_0 = 53 \text{ m/s}$, $\ddot{s}_0 = 2 \text{ m/s}^2$, $N_s = 6$, and $T = 4 \text{ s}$.

The relative trajectory generation can track the racing line if the vehicle velocity is close to the racing line velocity, but problems arise if the vehicle velocity deviates strongly from it. Specifically, reaching the racing line velocity is only possible with restrictions, as the course of the trajectories depends on the position on the race track. For example, at a section of the race track with a strong deceleration of the racing line, there may be no longitudinal curve with a monotonically increasing velocity profile, which prevents a proper approach to the racing line velocity at this location. To address this issue, we switch to the jerk-optimal generation for the longitudinal curves if $|\dot{s}_0 - \dot{s}_{r1}(0)| / \dot{s}_{r1}(0)$ exceeds a threshold $s_{0,\text{thr}}$. In the lateral direction, however, we use both the jerk-optimal and the relative curves. Thus, for every longitudinal profile $s_i(t)$, two lateral curves are generated for each sampled end position $n_{e,j}$. This increases the variety of maneuvers that can be planned, which is particularly advantageous for overtaking maneuvers.

After generating the curves in curvilinear coordinates, these are converted into Cartesian coordinates. Analogous to the derivation in [15], we perform the closed transformation $[s, \dot{s}, \ddot{s}, n, \dot{n}, \ddot{n}](t) \rightarrow [x, y, z, v, \hat{\chi}, \hat{a}_x, \hat{a}_y, \hat{\kappa}](t)$ for this. In contrast to [15], in which only 2D tracks are considered, the variables here refer to the newly introduced vehicle's velocity coordinate system on the 3D road plane. This velocity frame is obtained by rotating the road frame introduced in Section II-A around the $\mathbf{m}(s)$ axis (z-axis) by the angle $\hat{\chi}$ such that the x-axis is parallel to the projection of the absolute vehicle velocity onto the road plane v . The origin of the velocity coordinate system is formed by x , y , and z , representing the geometric center of the vehicle on the road plane. \hat{a}_x and \hat{a}_y are the accelerations in the x- and y-axis, while $\hat{\kappa}$ corresponds to the curvature on the road plane.

E. Feasibility Checks

We perform three checks on each generated trajectory to verify its feasibility. First, the path of the trajectory is examined to ensure that it remains within the track bounds, taking into account the vehicle geometry. To avoid a costly check in Cartesian coordinates, we carry out a simplified check in curvilinear coordinates with the vehicle width d_w :

$$n_r(s(t)) + \frac{d_w}{2} + d_s \leq n(t) \leq n_l(s(t)) - \frac{d_w}{2} - d_s. \quad (8)$$

The check is based on the assumption that the vehicle drives parallel to the reference line, which can be compensated for by adding a safety margin d_s . Secondly, as a kinematic condition, we check whether the minimal turning radius of the vehicle r_{\min} is complied with: $\hat{\kappa}(t) \leq 1/r_{\min} = \hat{\kappa}_{\max}$.

Lastly, compliance with the dynamic limits of the vehicle, i.e., the combined longitudinal and lateral acceleration, must be ensured. For an efficient check, we use gg-diagrams that constrain the combined accelerations of the vehicle and are calculated offline. These represent the complexity of a sophisticated dynamic vehicle model and are based on the quasi-steady-state assumption that each point along a trajectory corresponds to stationary circular motion without considering transient effects. While the gg-diagrams only depend on velocity v on 2D tracks, they can be extended for 3D tracks. For this purpose, we enhance the gg-diagrams by the dependence of the vertical acceleration \tilde{g} as in [19]. This acceleration depends on the vehicle's movement along the 3D track and may, therefore, deviate from the gravitational acceleration $g = 9.81 \text{ m/s}^2$. For the generation of the gg-diagrams, we follow the method introduced in [9], in which a computationally advantageous diamond-shaped underapproximation of the actual diagram shape is derived. An underestimation is necessary as the actual vehicle limits should not be exceeded. As in [20], the actual limit shape is obtained based on a double-track model and a Pacejka tire model. The diamond-shaped underapproximation is characterized by its vertices $\tilde{a}_{x,\min}(v, \tilde{g})$ and $\tilde{a}_{y,\max}(v, \tilde{g})$ as well as a shape factor $1 \leq p(v, \tilde{g}) \leq 2$. By varying p , the shape varies from a rhombus ($p = 1$) to an ellipse ($p = 2$). The final fourth parameter is $\tilde{a}_{x,\max}(v, \tilde{g})$, limiting the positive longitudinal acceleration, meaning no symmetry is given in the longitudinal direction. Overall, the check is carried out using inequalities (9a) to (9c), with the time arguments being neglected for reasons of clarity.

$$\tilde{a}_x \leq \tilde{a}_{x,\max}(v, \tilde{g}) \quad (9a)$$

$$|\tilde{a}_y| \leq \tilde{a}_{y,\max}(v, \tilde{g}) \quad (9b)$$

$$|\tilde{a}_x| \leq |\tilde{a}_{x,\min}(v, \tilde{g})| \left[1 - \left[\frac{|\tilde{a}_y|}{\tilde{a}_{y,\max}(v, \tilde{g})} \right]^{p(v, \tilde{g})} \right]^{\frac{1}{p(v, \tilde{g})}} \quad (9c)$$

Note that in these inequalities the apparent accelerations $\tilde{a}_x(t)$ and $\tilde{a}_y(t)$, which include the effect of the gravitational acceleration, are constrained instead of the accelerations $\hat{a}_x(t)$ and $\hat{a}_y(t)$ introduced in Section II-D. The correlations required for the evaluation of (9a) to (9c), neglecting the arguments, are

$$\begin{bmatrix} \tilde{a}_x \\ \tilde{a}_y \\ \tilde{g} \end{bmatrix} = \begin{bmatrix} \hat{a}_x + g(c_{\mu s_{\varphi}} s_{\hat{\chi}} - s_{\mu} c_{\hat{\chi}}) \\ \hat{a}_y + g(s_{\mu} s_{\hat{\chi}} + c_{\mu s_{\varphi}} c_{\hat{\chi}}) \\ \dot{w} - \hat{\omega}_y v + g(c_{\mu} c_{\varphi}) \end{bmatrix}. \quad (10)$$

Here, s_{\square} and c_{\square} are abbreviations for $\sin \square$ and $\cos \square$, and the terms negligible according to [9] are omitted. In addition, the time derivative of the vertical velocity $\dot{w} = \dot{n}\omega_x + n\dot{\omega}_x$ with $\omega_x = \Omega_x \dot{s}$ and the angular velocity $\hat{\omega}_y = (\Omega_y c_{\hat{\chi}} - \Omega_x s_{\hat{\chi}}) \dot{s}$ of the velocity frame appear. A full derivation of (10) is given in the appendix of [9].

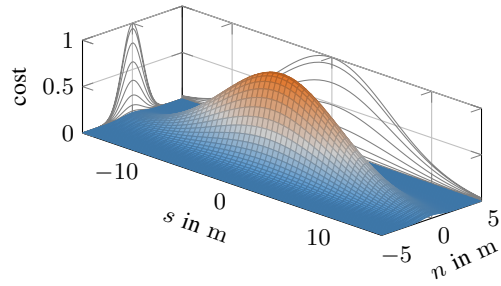


Fig. 5. Elliptical shaped prediction costs with $k_s = 0.015$ and $k_n = 0.5$ of an opposing vehicle located at $s_{\text{pr},m}(t) = n_{\text{pr},m}(t) = 0$.

Further, we apply a soft check concept for all three introduced checks. If all trajectories within a planning cycle are not feasible in one of the three checks, the trajectory with the fewest violations is selected. Consequently, a solution is always available that brings the vehicle into a viable state.

An essential aspect of the introduced checks is the consistency of the limits between the racing line and the local planning. To enable the racing line to be tracked, it must comply with the checks performed by the local planner. Moreover, a margin for the limits must be included in the local planning compared to the racing line, e.g., to provide additional acceleration potential needed for overtaking maneuvers. To realize this additional potential for local planning, we choose a larger safety margin $d_{s,\text{rl}} > d_s$ for the racing line in (8) and also scale the extremal values $\tilde{a}_{x,\min}(v, \tilde{g})$, $\tilde{a}_{x,\max}(v, \tilde{g})$ and $\tilde{a}_{y,\max}(v, \tilde{g})$ for the racing line in (9a) to (9c) with $1 - \tilde{a}_{\text{mgn}}$, where $\tilde{a}_{\text{mgn}} \in [0, 1)$.

Apart from the three checks, we do not perform a collision check with opposing vehicles. Instead, other vehicles are avoided due to an additional term in the cost function introduced in Section II-F. This is sufficient for the scenarios evaluated in this paper and has the advantage of a reduced computation time and that an infeasible state due to opposing vehicles within the safety distance is avoided.

F. Trajectory Selection

In the last step, costs are assigned to all feasible trajectories, and the cost-minimal trajectory is selected. The design of the cost function must be chosen so that the racing line is followed as closely as possible and, if necessary, other vehicles are avoided. This requires a prediction $(s_{\text{pr},m}(t), n_{\text{pr},m}(t))$, $t \in [0, T]$ for each considered opposing vehicle indexed with m , which is assumed to be given. The scalar total cost C of a specific edge is calculated by integration over time

$$C = \int_0^T w_n \cdot \Delta n^2(t) + w_v \cdot \frac{\Delta v^2(t)}{v_{\text{rl}}^2(t)} + w_{\text{pr}} \cdot d_{\text{pr}}(t) dt, \quad (11)$$

where the terms constitute a trade-off between racing line following and prediction avoidance, with $\Delta n(t) = n_{\text{rl}}(t) - n(t)$ and $\Delta v(t) = v_{\text{rl}}(t) - v(t)$. The parameters w_{\square} allow individual weighting of each term.

The first two terms penalize the lateral position deviation and the relative velocity deviation to the racing line, thereby

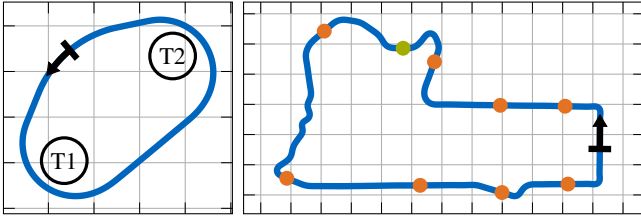


Fig. 6. Race tracks of LVMS (left) and MPCB (right). The arrows indicate the direction of travel and the respective $s = 0$ m position. The orange and green dots on the MPCB indicate the positions of the static objects mentioned in Section III-D. One grid cell equals 200 m in width and height.

achieving adherence to the racing line in the absence of opposing vehicles. The third term penalizes trajectories close to the prediction of the opposing vehicles, thus enabling overtaking maneuvers while maintaining a sufficient distance. $d_{\text{pr}}(t)$ is computed using the exponential expression

$$d_{\text{pr}}(t) = \sum_{m=0}^{M-1} e^{-k_s[s_{\text{pr},m}(t)-s(t)]^2 - k_n[n_{\text{pr},m}(t)-n(t)]^2}, \quad (12)$$

where M expresses the current number of opposing vehicles within the sensor range d_{snr} . It spans an elliptical shape around the predicted vehicle center, as depicted in Fig. 5. The shape is parameterized by k_s and k_n , which allows an overapproximation of the actual vehicle geometry and a safety distance. The ellipse has a maximum value of 1 in the geometric center of the vehicle and tends exponentially towards 0 as the distance increases. Due to the exponential progression, no sharp transition exists, preventing sudden changes in the trajectory planning between two planning cycles. In contrast to the cost design in [12], where also an elliptical shape is used, the ellipses in (12) are not aligned with the heading of the opposing vehicles due to the formulation in curvilinear coordinates. This prevents blockage of the entire track width by the cost ellipse, which may otherwise occur in the entry of sharp turns or due to uncertainties in the heading estimation of opponent vehicles.

III. RESULTS AND DISCUSSION

All experiments are conducted in simulations on the Las Vegas Motor Speedway (LVMS) and the Mount Panorama Circuit in Bathurst (MPCB), both depicted in Fig. 6. The LVMS is a 2400 m long oval race track with turns reaching a maximum banking of 20° enabling speeds of 90 m/s. The MPCB is 6250 m long and exhibits a more complex course. It has a maximum elevation difference of 175 m, a maximum slope of 13° , and a maximum banking of 8° . The choice of the respective reference line has a decisive influence on the overall behavior. For generated trajectories with a different orientation than the reference line, the velocity profile $v(t)$ is distorted compared to the specified $\dot{s}(t)$ profile, increasing the probability of non-feasibility. Since, in most cases, the racing line is followed or overtaking maneuvers of a similar orientation are performed, we choose the racing line to be driven as the reference line.

TABLE I
EXPERIMENT PARAMETERS

Parameter	Value	Parameter	Value
H_{rl}	500 m	\tilde{a}_{mgn}	0.1
T	3 s	w_n	0.1
N_s	40	w_v	100
K_s	1.2	w_{pr}	5000
N_n	15	k_s	0.015
$s_{0,\text{thr}}$	0.3	k_n	0.5
d_w	1.93 m	d_{snr}	200 m
d_s	0.2 m	N	30
$\hat{\kappa}_{\text{max}}$	0.1 m^{-1}	$\tilde{a}_{\text{abs,mgn}}$	0.8 m/s^2
$d_{s,\text{rl}}$	0.5 m	Δt_{sim}	0.1 s

A. Computational Details

The reference line \mathcal{C} and the track widths $n_l(s)$ and $n_r(s)$ are available as presampled curve points. For an evaluation between the discrete points, we rely on linear interpolation. The generated trajectories are represented by N equidistantly distributed discrete points in time, and the feasibility checks are performed only for these points. The offline-calculated extremal values and the shape factor for the representation of the gg-diagrams are stored as lookup tables for discrete v and \tilde{g} pairs and are interpolated online. Further, we approximate the cost function in (11) using the rectangle rule, with the N discrete points along the trajectory being used as integration points.

For racing line generation, we use the procedure proposed in [9]. It allows both the offline generation of a closed racing line for the entire race track and the online generation for the desired spatial horizon H_{rl} . Furthermore, it uses the same feasibility checks as in Section II-E, allowing the racing line to be traversed. The generated racing line is only available as discrete points and is evaluated at the needed N time points. However, due to the necessary interpolation, the resulting points may violate the feasibility checks, particularly affecting checks (9a) to (9c). If the absolute acceleration limits are low, the relative margin \tilde{a}_{mgn} introduced in Section II-E may not cover the violation, as the resulting surplus of permitted limits is also low. For this reason, we use an additional absolute margin $\tilde{a}_{\text{abs,mgn}}$, which guarantees a minimum margin regardless of the absolute limit values.

For simulation, an exact prediction of the opposing vehicles is utilized. The racing line generation, prediction, and local planning are executed sequentially, neglecting the effects resulting from different execution times. After a local planning cycle, the ego and the opposing vehicles are moved along the planned trajectory and prediction by a fixed time Δt_{sim} , ensuring a deterministic simulation.¹ All parameters used for the experiments are listed in Table I.

B. Relative Trajectory Generation

In the first experiment, we compare the performance for a flying solo lap using the jerk-optimal and the proposed

¹An implementation of the concept according to the stated details can be found in https://github.com/TUMRT/sampling_based_3D_local_planning.

TABLE II

LAP TIME COMPARISON USING DIFFERENT MOTION PRIMITIVES

#	Mode	Lap time in s	
		LVMS	MPCB
1	Offline racing line	27.12	125.96
2	Jerk-optimal trajectory generation	27.12	137.07
3	Relative trajectory generation	27.12	125.96

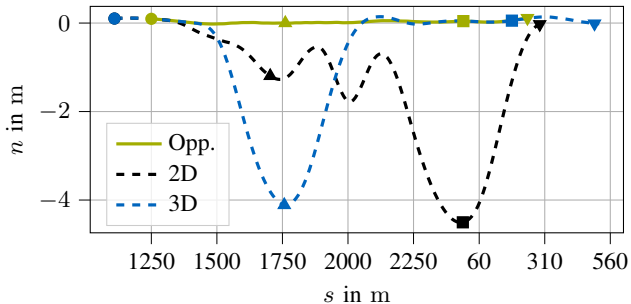


Fig. 7. Comparison of an overtaking maneuver on the LVMS in curvilinear coordinates using 2D and 3D friction checks. The opposing vehicle (Opp.) follows the racing line path ($n \approx 0$ m) at a constant speed of 70 m/s. Markers of the same shape represent the same point in time.

relative trajectory generation. Therefore, the objective is to follow the offline-calculated racing line without considering other vehicles. The resulting lap times compared with the lap time of the racing line are shown in Table II. While the lap time of the racing line is reached on the LVMS with both trajectory generation options, the lap time is significantly higher when using the jerk-optimal trajectory generation on the MPCB. This is due to the more complex track geometry of the MPCB and the associated racing line that the jerk-optimal trajectories cannot reproduce. Note that an entire lap without feasibility violations using the jerk-optimal edges on the MPCB is not possible, e.g., due to the poor racing line tracking and the correspondingly high speeds at turn entrances. Therefore, the soft check concept introduced in Section II-E becomes effective.

C. Planning in 2D and 3D

Including 3D effects enables the planning of driving maneuvers that would not be feasible in 2D. For comparison, we examine an exemplary scenario on the LVMS, in which an opposing vehicle drives on the racing line path at a constant speed of 70 m/s and is to be overtaken. This scenario is executed once considering the 3D effects and once assuming a flat 2D race track.

Fig. 7 shows the overtaking maneuvers performed for both cases in curvilinear coordinates. In the 3D case, the overtaking maneuver is performed at the first opportunity in turn T2. The banking of the turn causes an increase in \tilde{g} and thus also in the limits, which provides sufficient dynamic potential for the overtake. For the 2D case, however, a flat track ($\mu = \varphi = \Omega_x = \Omega_y = 0$) is assumed in the friction checks, which leads to $\tilde{a}_x = \hat{a}_x$, $\tilde{a}_y = \hat{a}_y$, and $\tilde{g} = g$ according to (10). This causes the limits to be underestimated

TABLE III

LAP TIME COMPARISON USING OFFLINE AND ONLINE RACING LINE

#	Mode	Lap time in s	
		LVMS	MPCB
1	Offline racing line (#1 in Table II)	27.12	125.96
2	Solo with offline racing line (#3 in Table II)	27.12	125.96
3	Solo with online racing line	27.17	126.13
4	Multi with offline racing line	27.74	128.38
5	Multi with online racing line	27.28	126.79

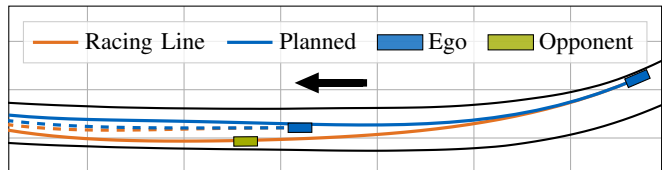


Fig. 8. Overtaking maneuver of a static obstacle (green dot in Fig. 6) with online racing line generation on the MPCB. The solid and dashed curves correspond to two different planning cycles over time.

in the turn, causing the opposing vehicle to be followed and the overtaking maneuver to be carried out on the main stretch after the turn. The lateral oscillations right before the maneuver result from planning differences within subsequent planning cycles due to the limited planning horizon.

In addition to neglected dynamic potential, shown exemplarily in this section, the acceleration limits can also be overestimated in the 2D case. This leads to a violation of the actual limits and occurs, e.g., when traversing a hill while $\Omega_y > 0$, resulting in $\tilde{g} < g$ and thus lower limits.

D. Online Racing Line Generation

With online racing line generation, the time-optimal trajectory for the finite spatial horizon H_{T1} is replanned from the current vehicle state in each planning cycle. We compare this approach with the use of an offline-calculated closed racing line that does not consider the current vehicle state.

First, we examine a flying solo lap that requires no deviation from the racing line. Entries #2 and #3 in Table III show the resulting lap times for the LVMS and MPCB. As already shown in Table II, when using the offline-generated racing line, the lap times of the racing lines can be retained for both tracks due to the relative trajectory generation. However, the lap times increase with the use of the online racing line generation, as the global time-optimal solution is not sufficiently approached due to the limited spatial horizon.

Subsequently, we consider flying laps while opposing vehicles occupy the racing line, forcing a deviation from it. On the LVMS, dynamic objects are placed every 200 m along the racing line, following it with 70% of the actual racing line speed. On the MPCB, we consider nine static objects placed along the offline-generated racing line, as depicted in Fig. 6. We choose static objects for the MPCB, as the difficulty of the overtaking maneuver varies depending on the position on the race track, and the use of fixed opponent

positions ensures reliable comparability of lap times. Entries #4 and #5 in Table III again list the lap times using the offline and online-generated racing lines. In contrast to solo driving, leveraging online racing line generation yields reduced lap times on both tracks. The higher lap times associated with the offline-generated racing line primarily result from necessary deviations from the racing line speed to facilitate overtaking maneuvers. This discrepancy arises since the trajectories generated to quickly guide the vehicle back to the global racing line speed are not feasible when approaching the vehicle's limits. In contrast, when using online racing line generation, a racing line is generated that brings the vehicle to the maximum speed in the shortest duration, considering the current state. Since the relative trajectory generation is based on this racing line, a return to maximum speed is faster than using offline racing line generation.

Fig. 8 illustrates an exemplary overtaking maneuver on the MPCB, showcasing the interplay between local trajectory planning and online racing line generation. In the first planning cycle considered, following the racing line would lead to a collision with the static object, causing an evasive maneuver to be planned. In the subsequent planning cycle, which is examined here, the time-optimal racing line corresponds to a shorter path. However, using the racing line generated offline would guide the vehicle away from the actual time-optimal line after overtaking, increasing the required time for this turn.

IV. CONCLUSION AND OUTLOOK

We have presented a sampling-based local trajectory planning approach for 3D race tracks. In contrast to existing approaches based on jerk-optimal edges, the proposed relative trajectory generation allows the lap time of the racing line to be maintained even for complex circuits. The 3D effects are incorporated by gg-diagrams that depend on the vertical acceleration and ensure that the dynamic potential is not exceeded or underestimated. Finally, we have demonstrated that online racing line generation, in combination with the local planner, slightly increases lap times in the solo scenario but can effectively reduce them for the multi-vehicle scenarios evaluated, especially on complex race tracks.

In the future, we will evaluate the proposed planning approach on a full-scale vehicle as part of the software stack of the TUM Autonomous Motorsport team. For this, the combination of local planner and control algorithm must be investigated with regard to the vehicle stability. Additionally, we will focus on greater maneuver diversity. This includes generating trajectories that differ from the jerk-optimal or relative trajectories to perform more complex maneuvers. It could also reduce the required margin of the limits between the sampling-based planner and the racing line generation. Another aspect is the addition of a second sampling stage, which would make it possible to plan outward and inward maneuvers within a single planning cycle. Finally, the effectiveness of online racing line generation should be investigated further. This could involve more complex scenarios and the use of alternative local planning approaches.

REFERENCES

- [1] A. Raji, A. Liniger, A. Giove, A. Toschi, N. Musiu, D. Morra, M. Verucchi, D. Caporale, and M. Bertogna, "Motion planning and control for multi vehicle autonomous racing at high speeds," in *2022 IEEE 25th International Conference on Intelligent Transportation Systems (ITSC)*. IEEE, 2022, pp. 2775–2782.
- [2] L. Ögretmen, M. Rowold, M. Ochsenius, and B. Lohmann, "Smooth trajectory planning at the handling limits for oval racing," *Actuators*, vol. 11, no. 11, p. 318, 2022.
- [3] L. Ögretmen, M. Rowold, T. Betz, A. Langmann, and B. Lohmann, "A hybrid trajectory planning approach for autonomous rule-compliant multi-vehicle oval racing," *SAE International Journal of Connected and Automated Vehicles*, vol. 7, no. 1, 2024.
- [4] L. Claussmann, M. Revilloud, D. Gruyer, and S. Glaser, "A review of motion planning for highway autonomous driving," *IEEE Transactions on Intelligent Transportation Systems*, vol. 21, no. 5, pp. 1826–1848, 2020.
- [5] J. Betz, H. Zheng, A. Liniger, U. Rosolia, P. Karle, M. Behl, V. Krovi, and R. Mangharam, "Autonomous vehicles on the edge: A survey on autonomous vehicle racing," *IEEE Open Journal of Intelligent Transportation Systems*, vol. 3, pp. 458–488, 2022.
- [6] F. Christ, A. Wischnewski, A. Heilmeier, and B. Lohmann, "Time-optimal trajectory planning for a race car considering variable tyre-road friction coefficients," *Vehicle System Dynamics*, vol. 59, no. 4, pp. 588–612, 2021.
- [7] A. Heilmeier, A. Wischnewski, L. Hermansdorfer, J. Betz, M. Lienkamp, and B. Lohmann, "Minimum curvature trajectory planning and control for an autonomous race car," *Vehicle System Dynamics*, vol. 58, no. 10, pp. 1497–1527, 2020.
- [8] I. Gundlach and U. Konigorski, "Modellbasierte online-trajektorienplanung für zeitoptimale rennlinien," *at - Automatisierungstechnik*, vol. 67, no. 9, pp. 799–813, 2019.
- [9] M. Rowold, L. Ögretmen, U. Kasolowsky, and B. Lohmann, "Online time-optimal trajectory planning on three-dimensional race tracks," in *2023 IEEE Intelligent Vehicles Symposium (IV)*. IEEE, 2023, pp. 1–8.
- [10] G. Jank, M. Rowold, and B. Lohmann, "Hierarchical time-optimal planning for multi-vehicle racing," in *2023 IEEE 26th International Conference on Intelligent Transportation Systems (ITSC)*. IEEE, 2023, pp. 2064–2069.
- [11] A. Liniger, A. Domahidi, and M. Morari, "Optimization-based autonomous racing of 1:43 scale rc cars," *Optimal Control Applications and Methods*, vol. 36, no. 5, pp. 628–647, 2015.
- [12] M. Rowold, L. Ögretmen, T. Kerbl, and B. Lohmann, "Efficient spatiotemporal graph search for local trajectory planning on oval race tracks," *Actuators*, vol. 11, no. 11, 2022.
- [13] S. M. LaValle, "Rapidly-exploring random trees: A new tool for path planning," Department of Computer Science, Iowa State University, Tech. Rep. 98-11, 1998.
- [14] A. Liniger and J. Lygeros, "A noncooperative game approach to autonomous racing," *IEEE Transactions on Control Systems Technology*, vol. 28, no. 3, pp. 884–897, 2020.
- [15] M. Werling, J. Ziegler, S. Kammel, and S. Thrun, "Optimal trajectory generation for dynamic street scenarios in a frenét frame," in *2010 IEEE International Conference on Robotics and Automation*. IEEE, 2010, pp. 987–993.
- [16] G. Perantoni and D. J. N. Limebeer, "Optimal control of a formula one car on a three-dimensional track—part 1: Track modeling and identification," *Journal of Dynamic Systems, Measurement, and Control*, vol. 137, no. 5, 2015.
- [17] A. Takahashi, T. Hongo, Y. Ninomiya, and G. Sugimoto, "Local path planning and motion control for agv in positioning," in *Proceedings. IEEE/RSJ International Workshop on Intelligent Robots and Systems '89. (IROS '89) 'The Autonomous Mobile Robots and Its Applications*, 1989, pp. 392–397.
- [18] M. Werling, S. Kammel, J. Ziegler, and L. Gröll, "Optimal trajectories for time-critical street scenarios using discretized terminal manifolds," *The International Journal of Robotics Research*, vol. 31, no. 3, pp. 346–359, 2012.
- [19] S. Lovato and M. Massaro, "A three-dimensional free-trajectory quasi-steady-state optimal-control method for minimum-lap-time of race vehicles," *Vehicle System Dynamics*, vol. 60, no. 5, pp. 1512–1530, 2022.
- [20] M. Veneri and M. Massaro, "A free-trajectory quasi-steady-state optimal-control method for minimum lap-time of race vehicles," *Vehicle System Dynamics*, vol. 58, no. 6, pp. 933–954, 2020.